Am J Nucl Med Mol Imaging 2024;14(3):182-188
www.ajnmmi.us /ISSN:2160-8407/ajnmmi0154100

Original Article

Fluoroestradiol PET-MRI imaging for detection of endometriosis lesions and symptom correlation

Jorge D Oldan[1], Yueh Z Lee[1], Kristen Olinger[1], Thad S Benefield[1], Erin T Carey[2], Noor D Abu-Alnadi[2], Steven L Young[2]

[1]Department of Radiology, University of North Carolina School of Medicine, 2000 Old Clinic, Campus Box 7510, Chapel Hill, NC 27599-7510, United States of America; [2]Department of Obstetrics and Gynecology, University of North Carolina School of Medicine, 4010 Old Clinic Building, Campus Box 7570, United States of America

Received October 25, 2023; Accepted February 23, 2024; Epub June 15, 2024; Published June 30, 2024

Abstract: Endometriosis is a common cause of infertility, pelvic pain, and dysmenorrhea and there are prior case reports of lesion detection using an 18F-fluoroestradiol (FES) tracer with positron emission tomography (PET). We aimed to further investigate the use of the FES tracer in the context of PET-magnetic resonance (PET-MR) imaging. We administered FES to 6 patients and then imaged them using a Siemens mMR PET-MR scanner. Each patient was taken to surgery within 30 days after imaging, and surgical visualization served as the gold-standard for diagnosis. PET did not prove to be as sensitive as MR (50% per-patient sensitivity versus 67% per-patient and 35% versus 48% per-lesion), and did not show any additional sites over and above MR. When MR was used to localize lesions on PET after imaging, there was insufficient evidence of an association between total tracer uptake and reported pain intensity (P=0.25). FES PET-MR offers no additional value to MR for endometriosis.

Keywords: Positron emission tomography, magnetic resonance imaging, imaging, endometriosis, pelvic pain

Introduction

Endometriosis is a chronic inflammatory disorder that affects approximately 1 in 10 reproductive-aged women [1, 2], and is a significant cause of both pelvic pain and infertility [3]. Endometriosis is diagnosed by the expression of estrogen-sensitive endometrial-like glands and stroma outside the uterus. Three clinical phenotypes of endometriosis have been described: superficial endometriotic implants on the peritoneum, endometriomas, and deeply infiltrating endometriosis (a nodule extending ≥5 mm beneath the peritoneum). Despite the disease prevalence, definitive diagnosis of endometriosis is often significantly delayed, with time between onset symptoms and diagnosis exceeding 5 years globally, and upper estimates 7-10 years [4].

This diagnostic delay in endometriosis is multifaceted. Endometriosis symptoms frequently overlap with other pain conditions (i.e. primary dysmenorrhea, irritable bowel syndrome, pelvic floor dysfunction) or simply present as infertility without significant pain. Imaging is often used in the investigation of chronic pelvic pain, however imaging sensitivity for endometriosis varies depending on the lesion phenotype and size, with early stage disease often undetectable by non-surgical approaches. There are also no reliable diagnostic biomarkers in blood or urine available. At present, visualization and/or histological examination of surgically-directed biopsies are the only usable diagnostic modality for the detection of stage 1 or stage 2 disease. As surgical intervention is associated with risk, empiric treatments of suspected disease are frequently utilized in clinical practice [5].

Even more advanced endometriosis and deeply infiltrating lesions can be difficult to diagnose preoperatively. While pelvic ultrasonography has the highest sensitivity and specificity in identifying ovarian endometriomas, it is not nearly as sensitive at the detection of deeply infiltrative or peritoneal lesions [2, 4]. Magnetic resonance imaging (MRI) also has high sensitivity and specificity for identifying ovarian endometriomas, but detection of superficial peritoneal endometriosis by MRI alone is often unachievable and adequate detection of deep infiltrating endometriosis (DIE) by US and/or MRI often requires specific training and approach. Cross-sectional imaging techniques, including computed tomography and magnetic resonance imaging (MRI) have limited utility in identifying endometriomas, though MRI has increased sensitivity and specificity in deeply infiltrative lesions and colonic disease [6]. Diagnostic delay compounded by the inability to identify and monitor early-stage lesions limits our ability to understand disease pathogenesis and progression as well as to monitor disease response to current therapeutic interventions and greatly limits the development of novel therapeutics.

Positron emission tomography (PET) offers the potential for a molecular-based imaging for highly specific diagnosis and monitoring of endometriosis. Endometriotic lesions, including endometriomas, express the estrogen receptors ERa and ERb, which bind specifically to estro-

https://doi.org/10.62347/JOQM7920

gen and estrogen analogs such as FES [7, 8]. This has already allowed the tracer to find a clinical role in the diagnosis of breast cancer, in finding previously more occult tumors like invasive lobular carcinoma [9], selecting patients for hormonal therapies, and assessing status in difficult-to-biopsy lesions [10]. The objective of our study was to evaluate the preoperative diagnostic performance of 18-fluoroestradiol (FES) for detecting endometriosis, compared to surgical staging and patient symptom severity.

Materials and methods

We conducted a single-site, prospective pilot study. The primary end point of the study was the feasibility of PET/MRI imaging with FES to identify endometriosis lesions and compared to diagnosis at surgery, the current gold standard.

Recruitment and surveys

Inclusion criteria were women aged 18-50 with suspected superficial or peritoneal endometriosis or extragenital DIE with the need for laparoscopic confirmation/resection as determined by the minimally invasive gynecologic surgery team. They also had to have a willingness to undergo experimental imaging. Exclusion criteria included the use of hormone treatments (combined oral contraceptives, progestins, gonadotropin releasing hormone analogs) for at least two cycles, or pregnancy/breastfeeding. Demographics were abstracted from the electronic medical record and patients completed the Endometriosis Health Profile-30 (EHP-30) [11]. A pain numeric rating scale (NRS) was collected and information about the last menstrual period were also obtained. Patients underwent FES PET/MRI (positron emission tomography/magnetic resonance imaging) within 30 days of the scheduled surgery and the surgical team was blinded to the imaging findings. Immediately postoperatively the surgeon completed the revised American Society for Reproductive Medicine (ASRM) classification of endometriosis form [12, 13]. Postoperatively, the imaging findings were compared to surgical staging and histopathologic specimens.

Imaging

PET images were obtained at 30 and 90 minutes after injection of 6 mCi of F-18 FES. Images were reconstructed to a 172×172 matrix at 4.2×4.2×4.2 cm using the ordered subset expectation maximization (OSEM) method at 3 iterations and 21 subsets.

MRI sequences included pelvic Half-Fourier Acquisition Single-Shot Turbo Spin Echo (HASTE) coronal, sagittal, and axial, HASTE axial Spectral Attenuated Inversion Recovery (SPAIR), pelvic T2-weighted high-resolution small-field-of-view sagittal, axial, and coronal, pelvic diffusion-weighted, pelvic T1 Volumetric Interpolated Breath-Hold (VIBE) fat-saturated axial, repeat pelvic HASTE coronal and axial fat-saturated, abdominal HASTE coronal, abdominal T1 VIBE coronal, pelvic T1 VIBE coronal, axial T1 VIBE fat-sat, axial T1 VIBE in and out of phase, and abdominal HASTE axial fat-saturated.

PET and MRI were interpreted separately by specialists in nuclear and abdominal imaging, respectively. A subsequent 'second pass' review of the imaging was performed to identify the SUVmax (the hottest pixel, a standard measure of intensity on PET) on the PET at the location of the MRI lesion even in the absence of a visible PET lesion, specifically on the T1 fat-saturated axial sequence. Images and lesions are available in the Supplementary Materials. To identify if lesion intensity had any relationship with symptoms, the maximum SUVmax (presumably representing the most aggressive lesion), or hottest lesion, and the average SUVmax (representing the average intensity, to avoid effects from the number of lesions) were correlated (using a standard Pearson correlation coefficient) with overall 30-symptom inventory, pain intensity, work symptoms, and sexual symptoms.

During the surgical procedure, the abdomen and pelvis were visually inspected using direct laparoscopic visualization. The surgeon methodically evaluated the reproductive organs, and all suspected areas were classified as either superficial peritoneal endometriosis or deep infiltrating endometriosis and with their anatomic location in the surgical record and completion of the ASRM endometriosis staging classification. This scoring was performed blinded to the PET and MRI results.

Statistics

Sensitivity, specificity, positive predictive value (PPV), negative predictive value (NPV), and overall accuracy were calculated for each imaging modality (MR or PET), both per-patient and per-lesion.

On a per-patient basis, sensitivity was defined as the number of patients who had endometriosis correctly identified on the modality in question (true positives), divided by the total number of patients who had endometriosis (true positives plus false negatives). PPV was defined as the number of patients who had endometriosis correctly identified on the scan (true positives), over the total number of patients with endometriosis identified on the scan. Specificity (true negatives over true negatives plus false positives) is undefined as there were no true negatives or false positives (all patients had endometriosis), but NPV (true negatives over true negatives plus false negatives) was zero as false negatives existed. Accuracy was equal to sensitivity as all patients had endometriosis. On a per-lesion basis, detection rate was defined as the percentage of all lesions found at surgery by either MR or PET.

To gain a reasonable estimate of specificity in a case where no patients completely lacked disease and each

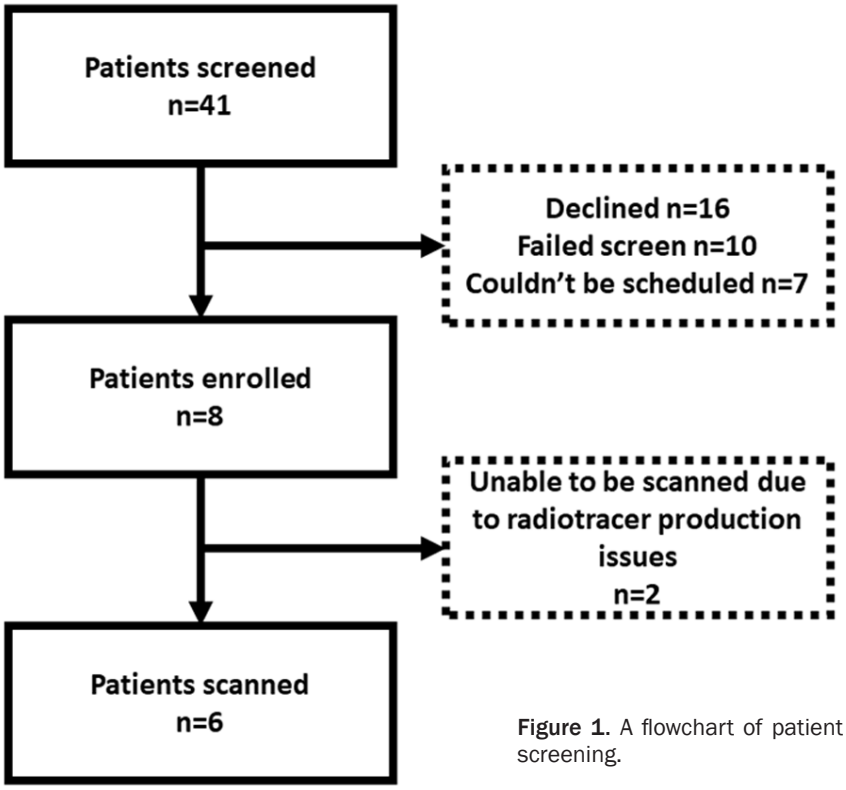

Figure 1. A flowchart of patient screening.

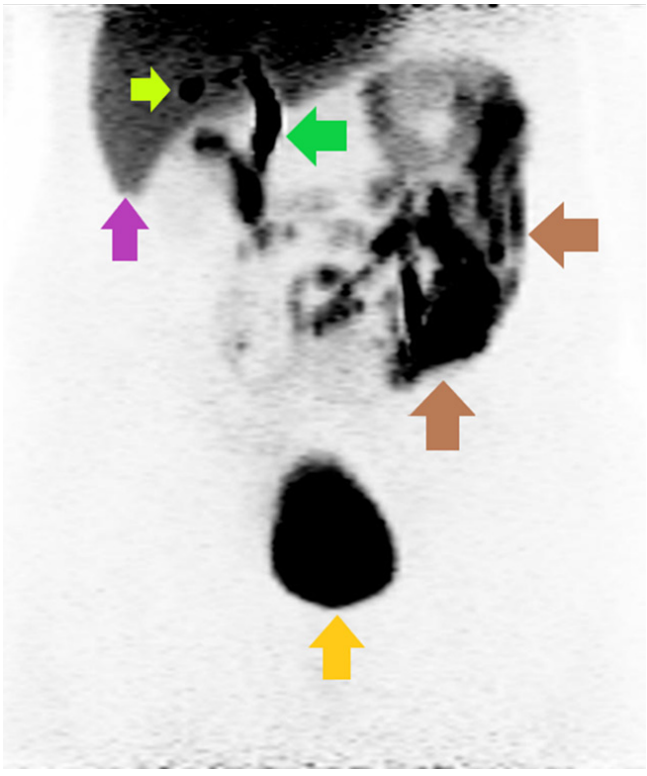

Figure 2. Maximum intensity projection of Patient 6, with tracer in bowel (brown arrows), liver (purple arrow), common bile duct (dark green arrow), gallbladder (light green arrow), and bladder (yellow arrow). Note intense bowel activity.

lesion could be in a different location in the peritoneum, a by-region approach was taken, using the regions given as part of the American Society of Reproductive Medicine (ASRM) endometriosis scoring system: right ovary, left ovary, posterior cul-de-sac, and remainder of the peritoneum.

On a per-lesion basis, sensitivity was defined as the number of correctly identified endometriotic lesions on the imaging modality (true positives) divided by the total number of endometriotic lesions at surgery (true positives + false negatives). Specificity was defined as the number of endometriotic lesions not identified at imaging (true negatives) divided by the total number of negative lesions (true negatives plus false negatives); since all patients had endometriosis this was undefined. PPV was calculated as the number of lesions identified at imaging and confirmed at surgery (true positives) divided by the total number of lesions identified at imaging (true positives + false positives); with no false positives this would be 100%. NPV was calculated as the number of true negatives divided by the number of negative results (true negatives + false negatives); again with multiple false negatives but no true negatives this is simply 0. Accuracy was calculated as the number of true positives plus true negatives (total correct number) divided by the total number of lesions studied. Sensitivity and accuracy by-patient and detection rate by-lesion were compared using McNemar's test. Statistical calculations were performed using SAS, Version 9.4.

To evaluate whether SUVmax is associated with the 30-point pain inventory scale, we implemented a mixed effects linear model. SUVmax was regressed on pain score, controlling for BMI and age. We included a random intercept term to account for within-patient correlations. A *p*-value of <0.05 for the pain inventory parameter estimate was considered evidence of an association. We also did a simple linear correlation with total lesion tracer uptake for the patient as a whole (as an index of disease burden). This study was approved by the University of North Carolina Institutional Review Board, IRB # 20-0328.

Results

41 patients were approached. Of these, 16 declined to participate, 10 failed various screens (most commonly being on birth control medications, but other exclusions such as metallic items in hips and becoming pregnant were also seen), and 7 were eligible but could not be scheduled, most commonly due to surgery being too soon or the cyclotron being unavailable due to maintenance. A final total of eight patients with symptomatic

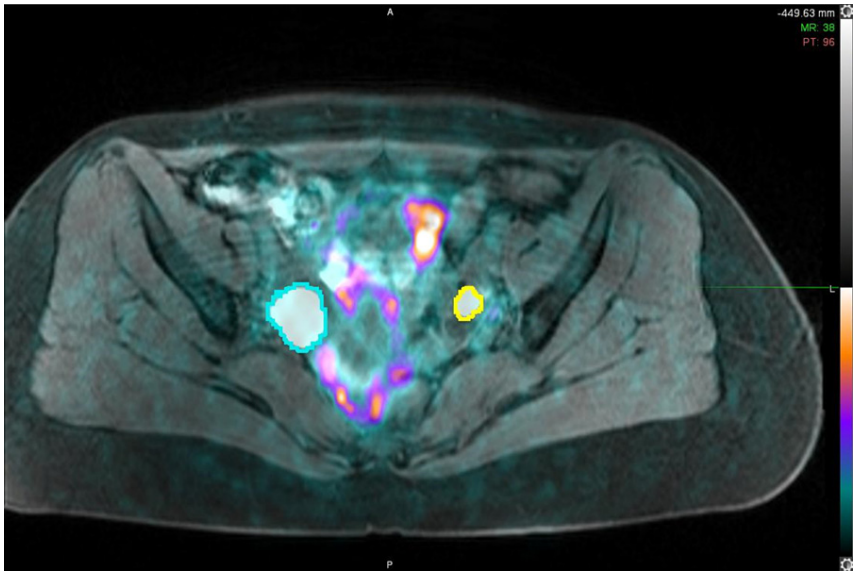

Figure 3. Patient 1. Mild diffuse uptake in endometriomas (yellow and blue outline). Uptake is lower than nearby bowel, complicating evaluation.

endometriosis were enrolled between August 2020 and July 2022 (**Figure 1**). Six of the patients completed the pilot protocol, with two unable to be scanned due to difficulties with tracer synthesis. Patients were of childbearing age between 27 and 49 years old (median age =32 years). Three patients had stage I/II and 3 had III/IV endometriosis according to the revised ASRM classification.

An example of a maximum intensity projection image of the abdomen and pelvis (the only area scanned) is given in **Figure 2**, showing the uptake in the bowel. Imaging findings by PET, MRI, and surgical findings are reported in **Tables 1** and **2**. **Table 3** gives sensitivity and NPV by-patient and by-region, as well as detection rate by-lesion (and PPV, which was always 100% as no patients were negative). Of note, the specificity of either MR or PET alone was 100%, but the sensitivity of MR appeared superior to that of PET alone, though this was not significant (P=0.317) on a per-patient or (P=0.242) on a per-region or per-lesion basis. The visible lesions appeared to be the larger cystic and DIE lesions, while the peritoneal lesions were not localized by either PET or MR. There was no lesion visible on PET that was not also identified on MR.

We also examined the data for correlation between tracer uptake and symptoms. **Table 4** shows the values of SUVmax and EHP-30 findings. In general, the results suggested a relationship between lesion avidity for the tracer and symptoms. Patients 1 (**Figure 3**) and 6 (**Figure 4**) had the most avid lesions and the worst symptoms, whereas patient 5 had a large volume of disease at surgery but relatively mild symptoms and relatively low uptake. Patients 2 and 8 had relatively mild symptoms, imaging findings, and ultimately less disease. Patient 3 was something of an outlier, with extensive disease not noted on MR or PET. The mixed-effects linear model suggested no association between higher pain scores and higher SUVmax, but there was at least some weak linear association between total lesion tracer uptake and pain score (P=0.25).

Discussion

The PET/MR imaging of suspected endometriosis lesions was highly specific compared to the surgical findings, however, relatively low sensitivity for both modalities (on both per-patient and per-lesion basis), with no significant diagnostic improvement over existing technology. PET was less sensitive than MR (50% vs 67% by-patient and 35% vs 48% detection rate by-lesion), and demonstrated no additional lesions. In our pilot study, we did not find that the addition of PET imaging (with or without comparison with MRI) provides greater diagnostic benefit over MRI.

Additionally, some lesions, not identifiable prospectively on PET, were retrospectively identifiable using MRI; many of these had SUVmax below the usual cutoff of 2.5 used for malignancy, and in any case would not be likely to be identifiable without MRI. We also found that many smaller lesions (<1 cm) were not detectable at all. This is already a known limitation in MRI, where superficial disease, characteristic of stage 1 and 2, and DIE lesions <1 cm are not routinely visualized on imaging. While nuclear medicine scans can detect cancer lesions too small to find by MRI or CT (specifically lymph nodes under 1 cm), this was not seen in our study of endometriosis lesions using FES tracer.

The limitations of the present study include the small sample size. Challenges in recruitment were noted as patients were required to be off hormone therapy for greater than two cycles prior to imaging. We were underpowered to detect an association between SUVmax and pain as well as to formally compare performance measures by modality. A possible future avenue of investigation might be imaging after diuresis; this was difficult to consent patients for, but might be a possibility if patients are willing.

Some of the reason for the low sensitivity may be due to differences in isoforms of the estrogen receptor. There are two forms of the receptor, alpha and beta, and both eutopic endometrium and endometriosis show higher levels of mRNA for alpha than beta [14]; also, the affinity of 18F-FES is 6.3 times higher for the alpha than for the beta receptor [15]. However, the ER-alpha: ER-beta ratio is lower in endometriomas than it is in eutopic endome-

Table 1. Findings by PET and MR compared to surgery

Pt	MR	PET (first pass)	Surgical
1	L endometrioma (2.4); post cul-de-sac (2); R endometrioma (5.2)	Neg	Ant cul-de-sac at border of L bladder peritoneum; Deep infiltrating endometriosis peritoneum along b/l uterosacral ligs; R endometrioma w/dense adhesions; L endometrioma w/dense adhesions; Post cul-de-sac partial obliteration
2	Pararectal deposit (4.3)	Post cul-de-sac (pararectal)	Along anterior sigmoid colon w/att to L pelvic sidewall; L pararectal space
3	Neg	Neg	Appendix; Ant cul-de-sac peritoneum; L ant pelvic peritoneum; R ant pelvic sidewall peritoneum; L uterosacral ligament
5	Endometrioma (1) Ant cul-de-sac x2 (0.9, 2)	Adnexa Ant cul-de-sac	R endometrioma; R-sided diaphragmatic studding; L allen-masterson window of ant cul-de-sac
6	Adenomyosis (5.1); Endometrioma (4.3); Post serosal margin of uterus (2.4)	Adenomyosis; Post serosal margin of uterus; L adnexa; hematosalpinx	Adenomyosis; L endometrioma; L pelvic sidewall peritoneum; Post cul-de-sac obliteration; Gunpowder lesions across ant cul-de-sac, bladder, pelvic sidewall
8	Neg	Neg	Mild inflammatory lesions uterus

Patients 4 and 7 could not be imaged due to difficulties with tracer synthesis. SUVmax of lesions identified on MRI is given in parentheses; note that some lesions were not visible until reexamination on 'second pass'. Hematosalpinx was ignored as it is not normally detectable by surgery without incising the tube. Gunpowder lesions on patient 6 were counted as 1 finding.

Table 2. Surgical and ASRM scores

Pt	Surgical	ASRM score
1	Ant cul-de-sac at border of L bladder peritoneum; Deep infiltrating endometriosis peritoneum along b/l uterosacral ligs; R endometrioma w/dense adhesions; L endometrioma w/dense adhesions; Post cul-de-sac partial obliteration	Peritoneum, superf + deep (4+6) R ovary, deep (16) + dense adhesions (4) L ovary, deep (16) + dense adhesions (4) Posterior cul-de-sac obliteration (4)
2	Along anterior sigmoid colon w/att to L pelvic sidewall; L pararectal space	Peritoneum, deep (4)
3	Appendix; Ant cul-de-sac peritoneum; L ant pelvic peritoneum; R ant pelvic sidewall peritoneum; L uterosacral ligament	Peritoneum, superf + deep (4+6)
5	R endometrioma; R-sided diaphragmatic studding; L allen-masterson window of ant cul-de-sac	Peritoneum, superf + deep (4+4) R ovary, deep (20) + filmy adhesions (1) L ovary, superf (1) + filmy adhesions (1) R tube, filmy adhesions (1)
6	Adenomyosis; L endometrioma; L pelvic sidewall peritoneum; Post cul-de-sac obliteration; Gunpowder lesions across ant cul-de-sac, bladder, pelvic sidewall	Peritoneum, superf + deep (4+4) L ovary superf + deep (2+20) + dense adhesions (8) R ovary dense adhesions (8) Post cul-de-sac (4)
8	Mild inflammatory lesions uterus	Peritoneum, superf (1)

trium (5.2 versus 15.5) [16]. Given that the uptake of FES in endometriosis appears to be lower than that in eutopic endometrium, and uptake is relatively low compared to the liver, biliary system, bowel, and bladder as shown below, this might explain the relatively low levels of uptake. Thus, a future area of research might be the use of an FES ligand specialized for the ER-beta receptor.

Major strengths of the study are its prospective approach, the surgical experience of the team, and the study taking place at a single institution with a standardized clinical approach to the evaluation of endometriosis.

Conclusions

FES-PET does not show any significant ability to detect specific deposits of endometriosis over and above MRI;

Table 3. Sensitivity by-patient and by-region, detection rate by-lesion, PPV, and NPV by-patient and by-region

Modality	Sensitivity, by-patient	Sensitivity, by-region	Detection rate, by-lesion	PPV	NPV, by-patient	NPV, by-region
MR	67% (4/6)	67% (8/12)	48% (11/23)	100	0	80% (12/15)
PET	50% (3/6)	41% (5/12)	35% (8/23)	100	0	61% (11/18)

Table 4. Overall endometriosis health profile 30-point symptom inventory, with pain description, work symptom inventory, and sex symptom inventory

Patient	BMI	Age	SUVmax of lesions	Total tracer uptake	30-point symptom inventory	Pain description	Work symptom inventory	Sex symptom inventory
1	26.3	31.7	5.2, 2.4, 2	21.66	83	68	13	4
2	34	49.2	4.3	0.75	15	10	n/a	7
3	20.4	38.3	0	0	63	0	8	11
5	25.8	29.3	1, 0.9, 2	8.75	23	1	0	n/a
6	29	43.7	5.1, 4.3, 2.4	50.36	64	1	9	n/a
8	31.6	30.2	0	0	20	1	0	4

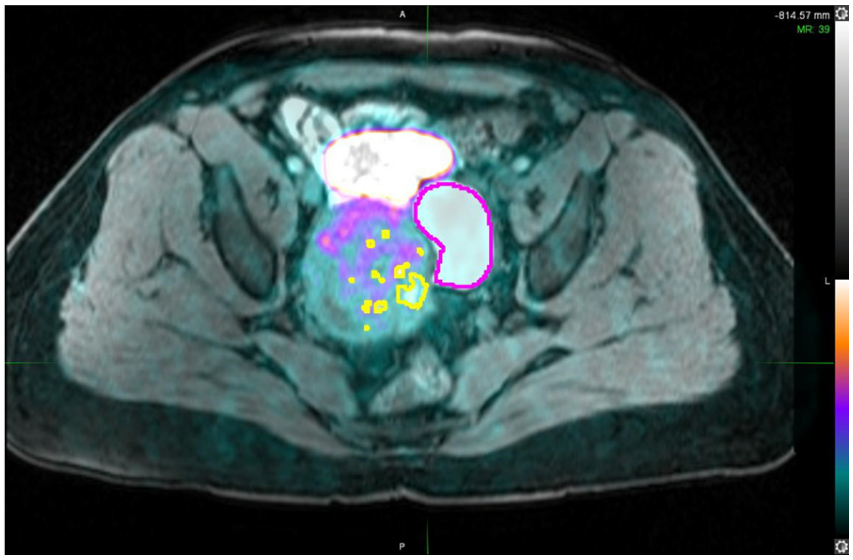

Figure 4. Patient 6. Diffuse low-level uptake in adenomyotic lesions (outlined in yellow) and large endometrioma (outlined in purple). Heterogeneous uptake does not clearly correlate to adenomyotic lesions, although the spatial resolution of PET is likely insufficient to evaluate this.

there is a correlation with pain intensity, but this does not reach the level of significance.

Acknowledgements

The project was supported by the National Center for Advancing Translational Sciences (NCATS), National Institutes of Health, through Grant Award Number 550KR231919. Also received support from the Eunice Kennedy Shriver NICHD/NIH, Grant Award Number P01HD106485. The content is solely the responsibility of the authors and does not necessarily represent the official views of the NIH.

Disclosure of conflict of interest

None.

Address correspondence to: Dr. Jorge D Oldan, Department of Radiology, University of North Carolina School of Medicine, 101 Manning Drive #B114, Chapel Hill, NC 27599, United States of America. Tel: 917-297-3687; E-mail: joldan9@gmail.com; Jorge_oldan@med.unc.edu

References

[1] Vander Borght M and Wyns C. Fertility and infertility: definition and epidemiology. Clin Biochem 2018; 62: 2-10.

[2] Pascoal E, Wessels JM, Aas-Eng MK, Abrao MS, Condous G, Jurkovic D, Espada M, Exacoustos C, Ferrero S, Guerriero S, Hudelist G, Malzoni M, Reid S, Tang S, Tomassetti C, Singh SS, Van den Bosch T and Leonardi M. Strengths and limitations of diagnostic tools for endometriosis and relevance in diagnostic test accuracy research. Ultrasound Obstet Gynecol 2022; 60: 309-327.

[3] Parazzini F, Esposito G, Tozzi L, Noli S and Bianchi S. Epidemiology of endometriosis and its comorbidities. Eur J Obstet Gynecol Reprod Biol 2017; 209: 3-7.

[4] Exacoustos C, Manganaro L and Zupi E. Imaging for the evalution of endometriosis. Best Pract Res Clin Obstet Gynaecol 2014; 28: 655-81.

[5] Becker CM, Bokor A, Heikinheimo O, Horne A, Jansen F, Kiesel L, King K, Kvaskoff M, Nap A, Petersen K, Saridogan E, Tomassetti C, van Hanegem N, Vulliemoz N and Vermeulen N; ESHRE Endometriosis Guideline Group. ESHRE guideline: endometriosis. Hum Reprod Open 2022; 2022: hoac009.

[6] Bazot M, Bornier C, Dubernard G, Roseau G, Cortez A and Daraï E. Accuracy of magnetic resonance imaging and rectal endoscopic sonography for the prediction of location of deep pelvic endometriosis. Hum Reprod 2007; 22: 1457-63.

[7] Liao GJ, Clark AS, Schubert EK and Mankoff DA. 18F-fluoroestradiol PET: current status and potential future clinical applications. J Nucl Med 2016; 57: 1269-75.

[8] Cosma S, Salgarello M, Ceccaroni M, Gorgoni G, Riboni F, La Paglia E, Danese S and Benedetto C. Accuracy of a new diagnostic tool in deep infiltrating endometriosis: positron emission tomography-computed tomography with 16α-[18F]fluoro-17β-estradiol. J Obstet Gynaecol Res 2016; 42: 1724-33.

[9] Ulaner GA, Jhaveri K, Chandarlapaty S, Hatzoglou V, Riedl CC, Lewis JS and Mauguen A. Head-to-head evaluation of 18F-FES and 18F-FDG PET/CT in metastatic invasive lobular breast cancer. J Nucl Med 2021; 62: 326-31.

[10] Ulaner GA. 16α-18F-fluoro-17β-fluoroestradiol (FES): clinical applications for patients with breast cancer. Semin Nucl Med 2022; 52: 574-83.

[11] Jones G, Kennedy S, Barnard A, Wong J and Jenkinson C. Development of an endometriosis quality-of-life instrument: the endometriosis health profile-30. Obstet Gynecol 2001; 98: 258-64.

[12] Revised American Society for Reproductive Medicine classification of endometriosis: 1996. Fertil Steril 1997; 67: 817-21.

[13] Johnson NP, Hummelshoj L, Adamson GD, Keckstein J, Taylor HS, Abrao MS, Bush D, Kiesel L, Tamimi R, Sharpe-Timms KL, Rombauts L and Giudice LC; World Endometriosis Society Sao Paulo Consortium. World Endometriosis Society consensus on the classification of endometriosis. Hum Reprod 2017; 32: 315-24.

[14] Matsuzaki S, Murakami T, Uehara s, Canis M, Sasano H and Okamura K. Expression of estrogen receptor alpha and beta in peritoneal and ovarian endometriosis. Fertil Steril 2001; 75: 1198-205.

[15] Yoo J, Dence CS, Sharp TL, Katzenellenbogen JA and Welch MJ. Synthesis of an estrogen receptor beta-selective radioligand: 5-[18F]fluoro-(2R,3S)-2,3-bis(4-hydroxyphenyl)pentanenitrile and comparison of in vivo distribution with 16alpha-[18F]fluoro-17beta-estradiol. J Med Chem 2005; 48: 6366-78.

[16] Brandenberger AW, Lebovic DI, Tee MK, Ryan IP, Tseng JF, Jaffe RB and Taylor RN. Oestrogen receptor (ER)-alpha and ER-beta isoforms in normal endometrial and endometriosis-derived stromal cells. Mol Hum Reprod 1999; 5: 651-5.

Supplementary Materials

Patient 1

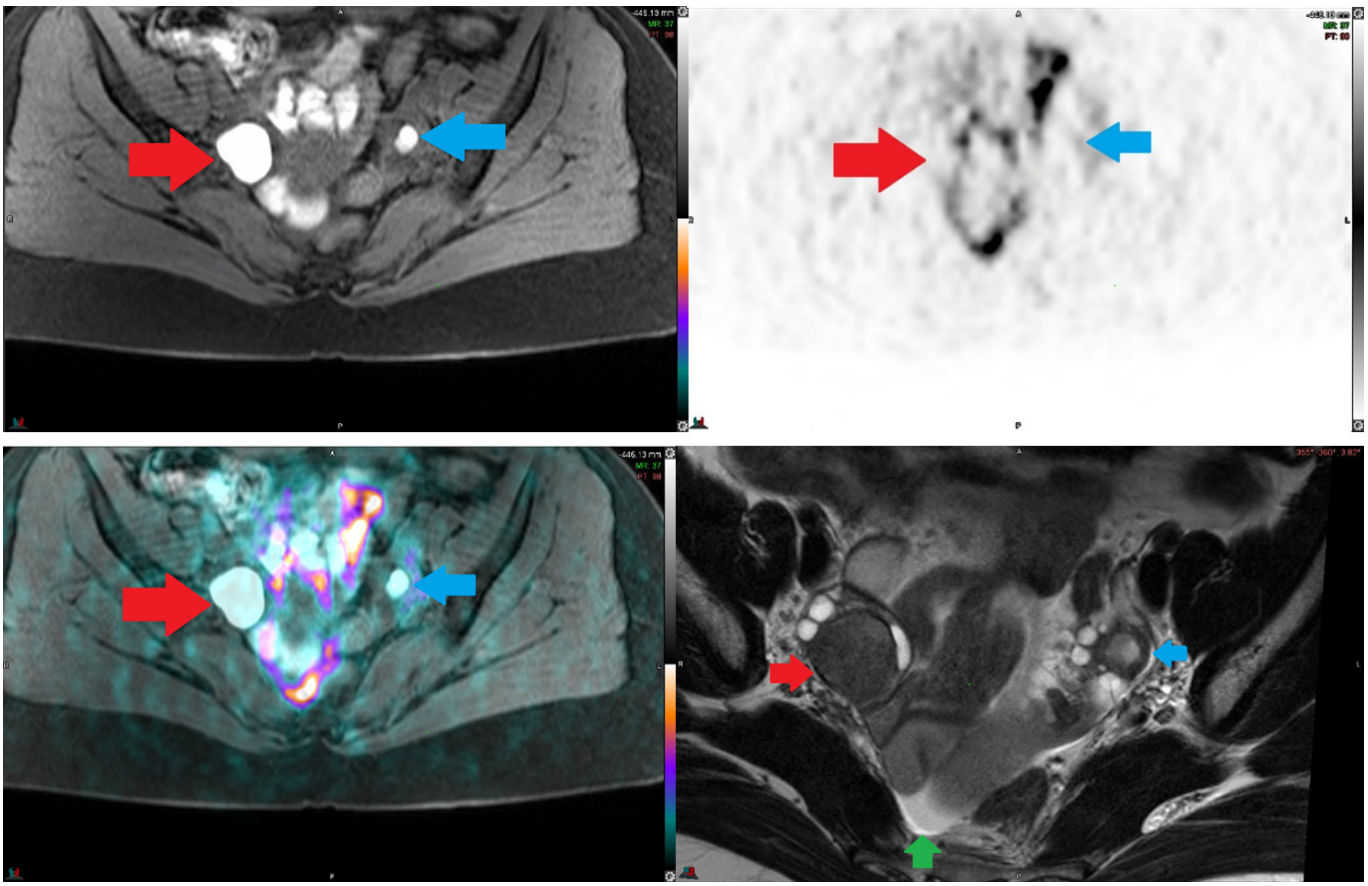

Clockwise from top left: T1 (fat-saturated), PET, T2 (high-resolution), and T1 fused images of right endometrioma (red arrow), left endometrioma (blue arrow), and posterior cul-de-sac deposit (green arrow). Note that due to differences in technique between T1 and T2 acquisitions, the posterior cul-de-sac deposit is only seen on the T2; it is demonstrated on the other sequences below.

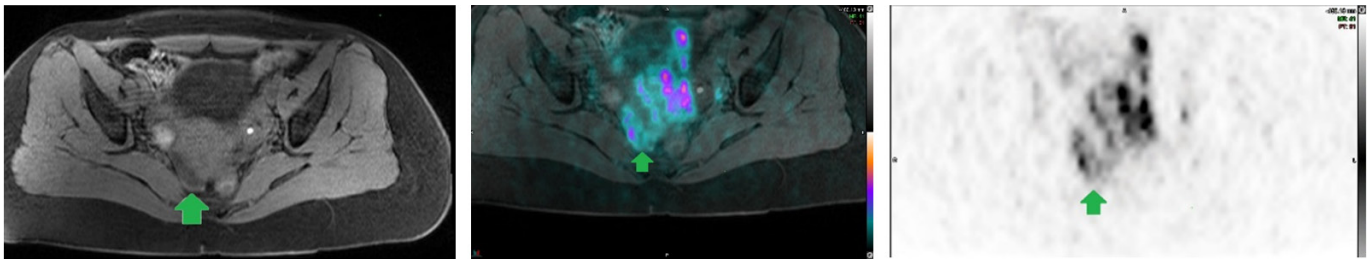

Left to right: T1 (fat-saturated), T1 fused, and PET images of posterior cul-de-sac deposit (green arrow).

Patient 2

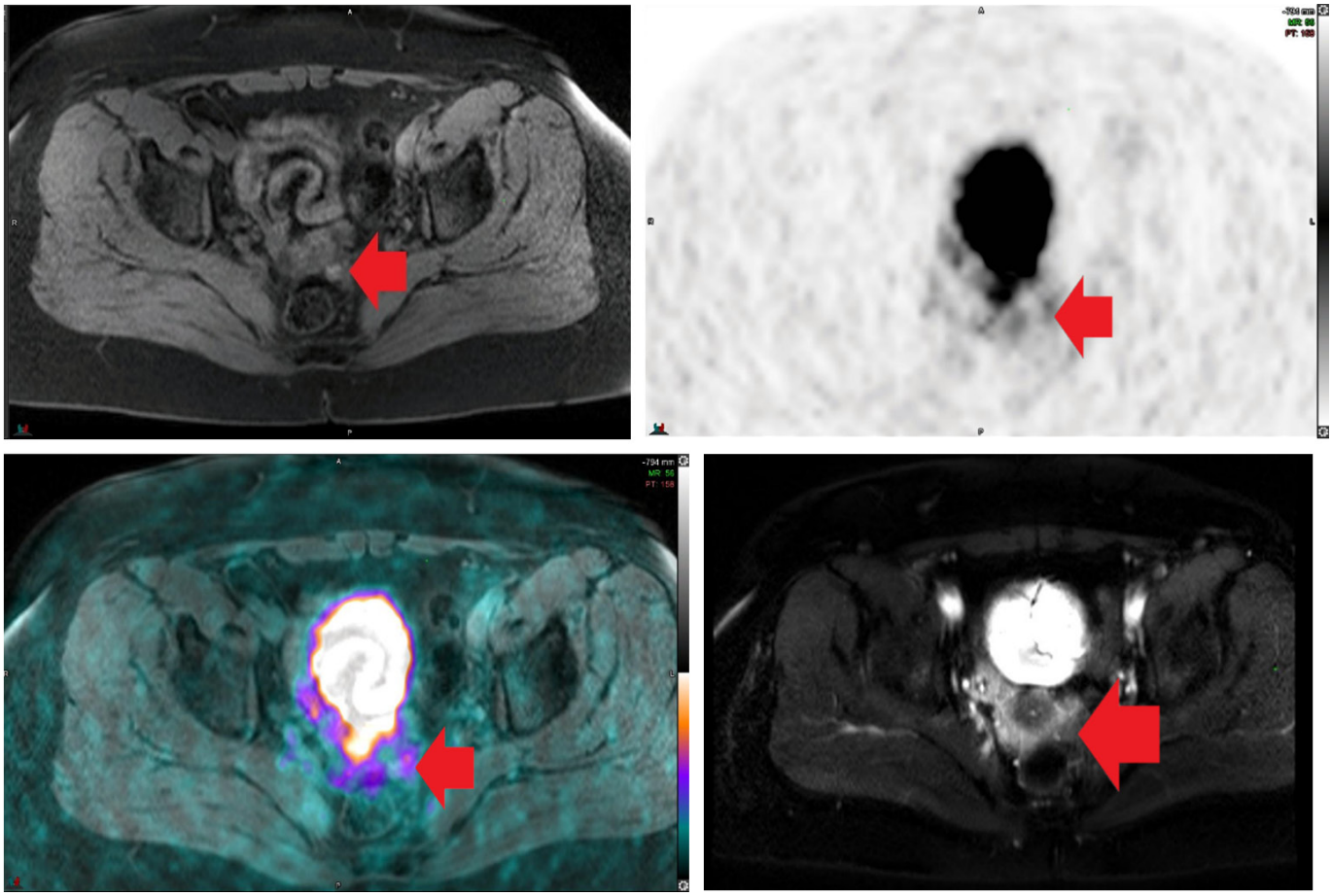

Clockwise from top-left: T1 (fat-saturated), PET, T2 (fat-saturated), and T1 fused images of the endometriotic deposit (red arrow).

Patient 5

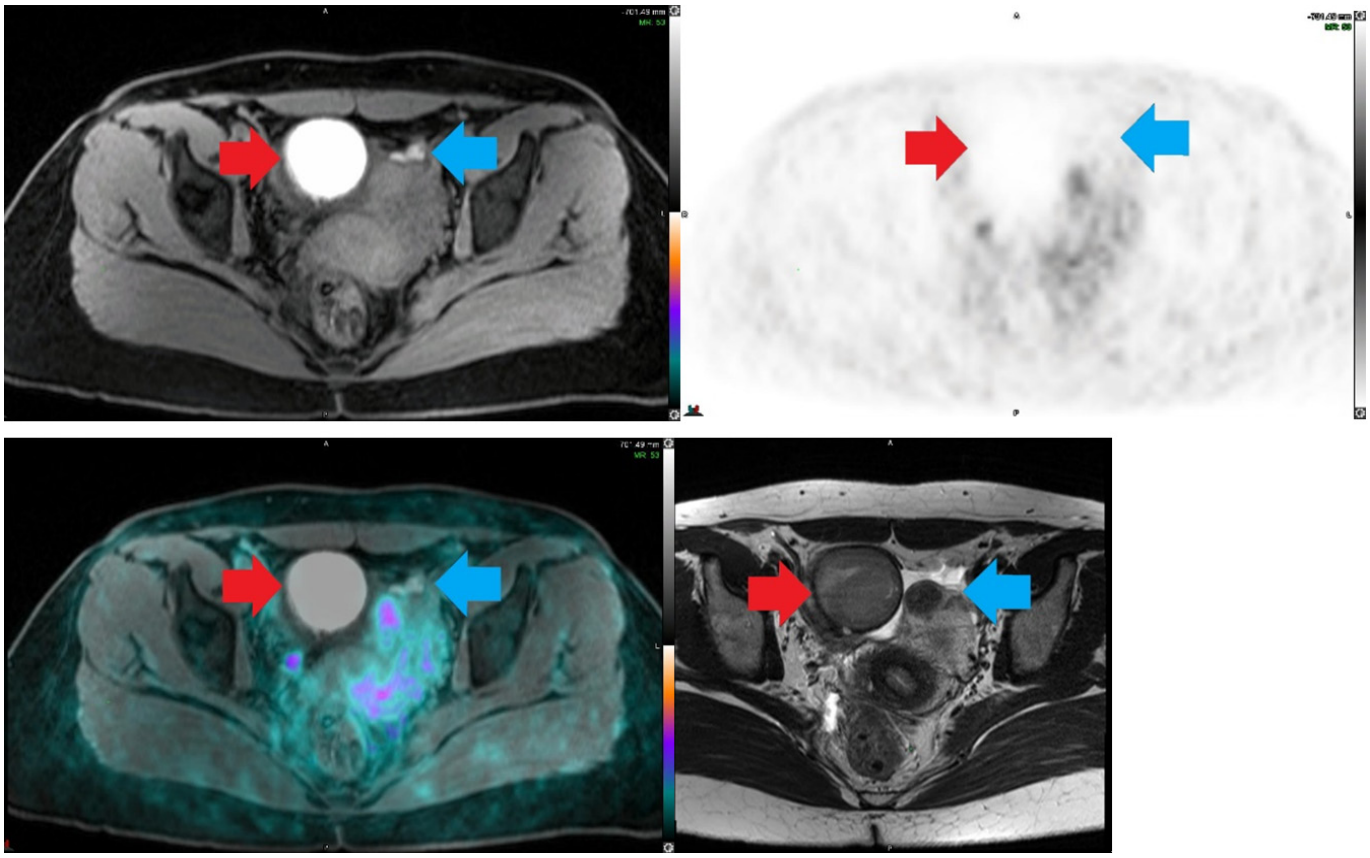

Clockwise from top left: T1 (fat-saturated), PET, T2 (high-resolution), and T1 fused images of right endometrioma (red arrow) and large anterior cul-de-sac deposit (blue arrow).

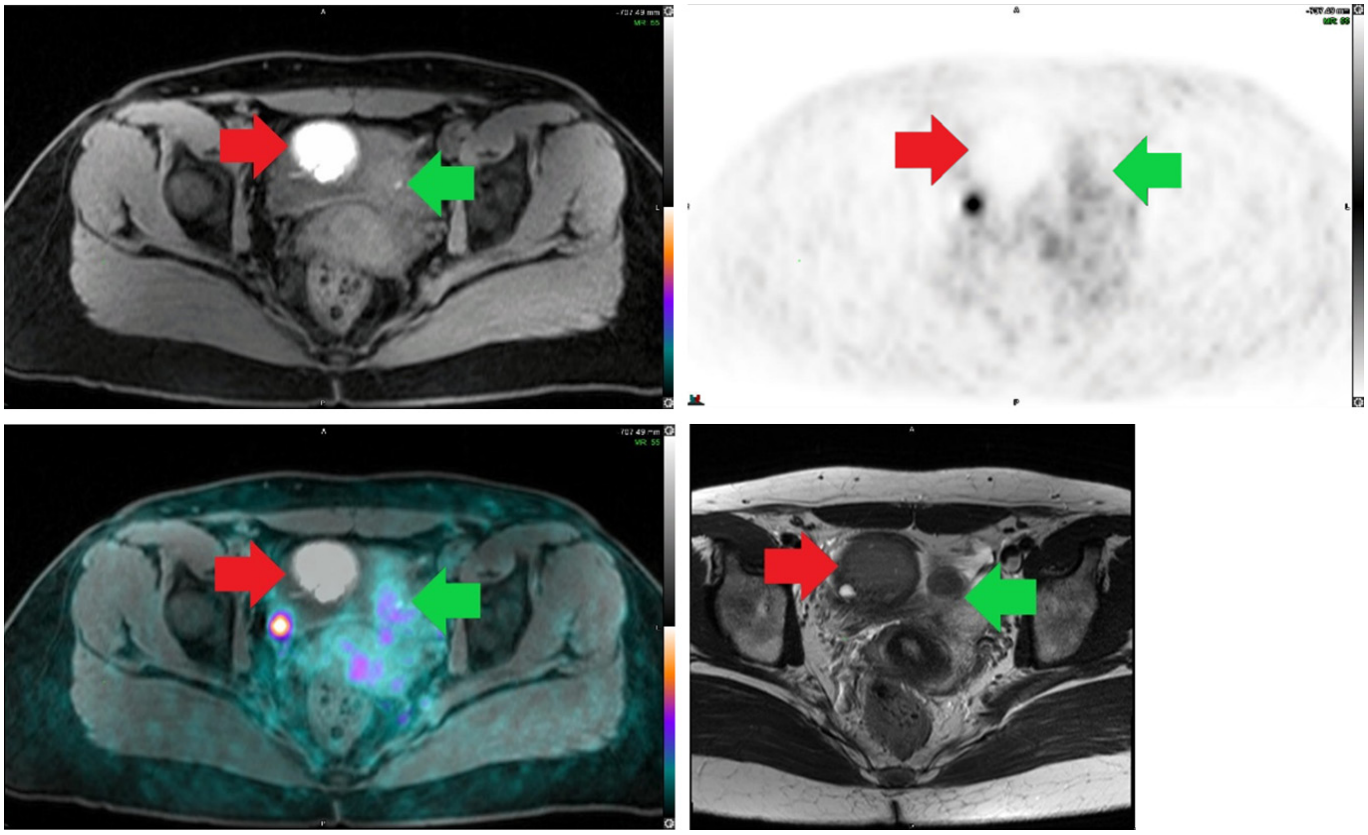

Clockwise from top left: T1 (fat-saturated), PET, T2 (high-resolution), and T1 fused images of right endometrioma (red arrow) and small anterior cul-de-sac deposit (green arrow).

Patient 6

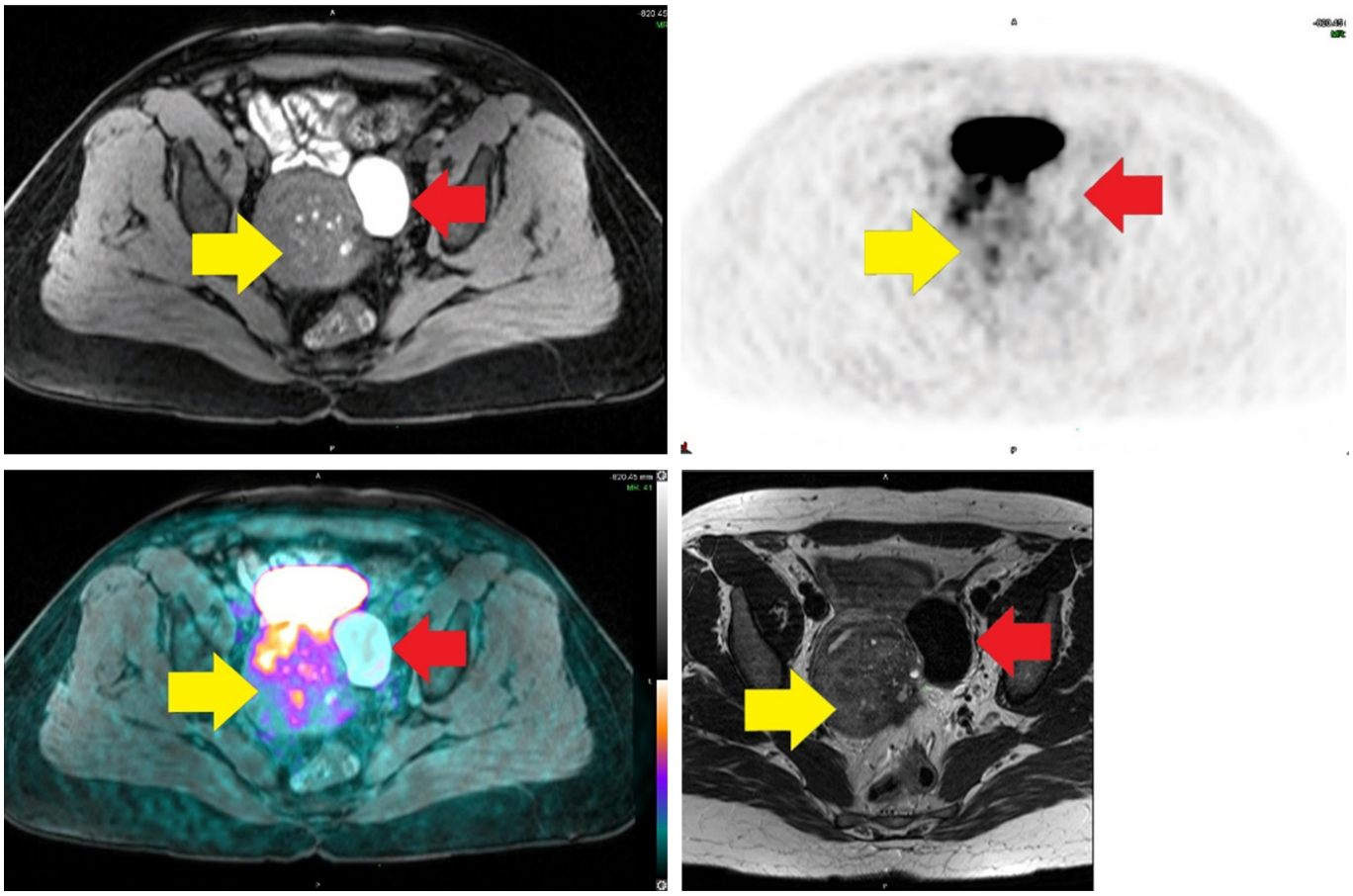

Clockwise from top left: T1 (fat-saturated), PET, T2 (high-resolution), and T1 fused images of left endometrioma (red arrow) and adenomyotic uterus (yellow arrow).

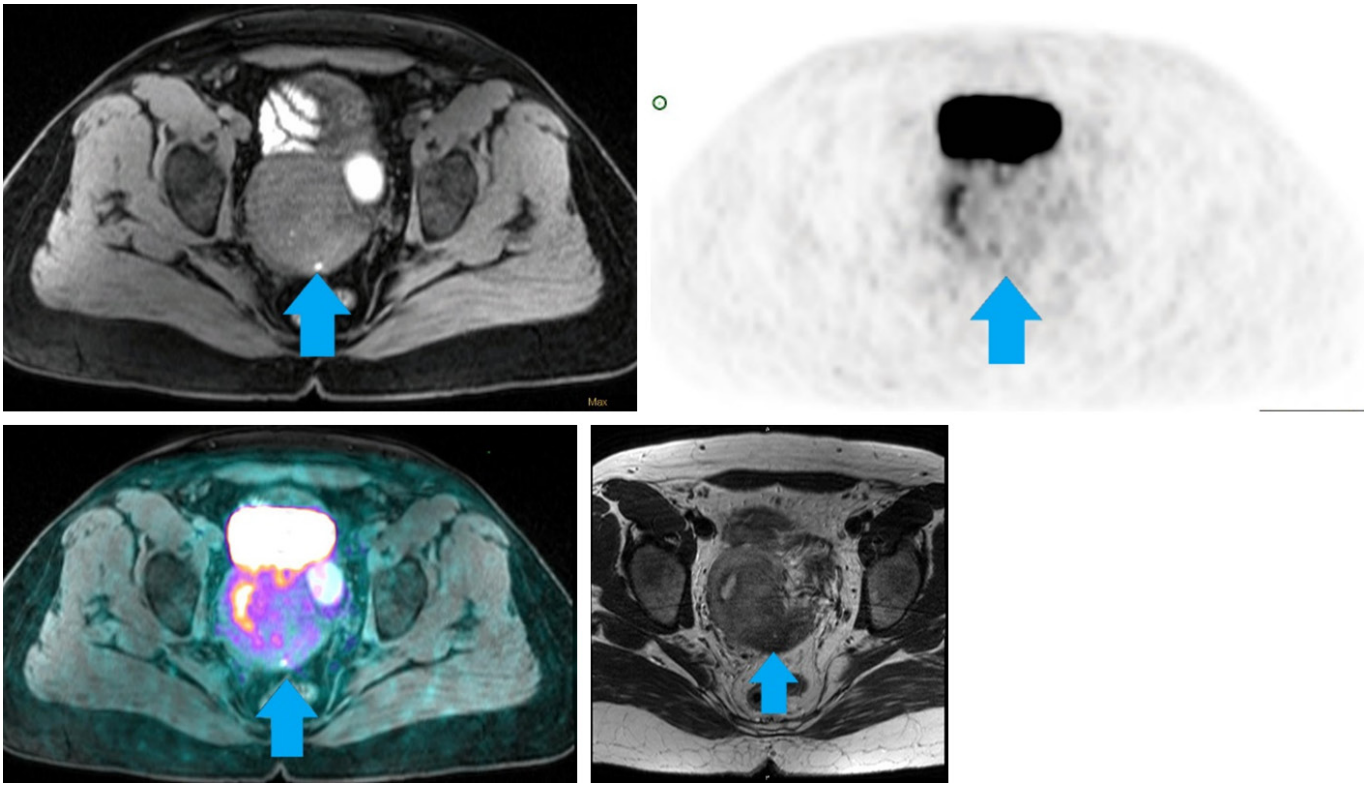

Clockwise from top left: T1 (fat-saturated), PET, T2 (high-resolution), and T1 fused images of posterior cul-de-sac deposit (blue arrow).

Patients 3 and 8 have no visible lesions on PET, as previously discussed. Patients 4 and 7 could not be scanned.